Techno-Science Research Journal V13 (2) (2025) P 23-32

Content list available at ITC

Techno-Science Research Journal

Journal Homepage: http://techno-srj.itc.edu.kh/

Techno-Science Research Journal

Low-Complexity Detection of Primary Synchronization Signal for 5G New Radio Terrestrial Cellular System

Leakana Ouk*, Rothna Pec, Sopkeaktra Chhorn

Department of Telecommunication and Network Engineering, Institute of Technology of Cambodia, Russian Federation Blvd., P.O. Box 86, Phnom Penh, Cambodia

Received:15 August 2024; Revised: 11 September 2024; Accepted: 13 September 2024; Available online: 30 August 2025

Abstract: *5G mobile communication is based on three main pillars: enhanced mobile broadband, massive machine-type communication, and ultra-reliable low latency. For a mobile station (MS) to connect to a 5G network and access user data, it must first perform cell identification during the initial stage before establishing radio and network connections. This is done using the primary synchronization signal (PSS) and secondary synchronization signal (SSS) sent out by the 5G base station (gNB). Because of movement, the Doppler effect, and battery limits on the MS, detecting PSS and SSS needs to be both strong and efficient. The parameters estimated in this process include timing, carrier frequency offset, cell ID, and numerology. This paper looks at a cell identification technique that works well for an MS, introduces a low-complexity PSS detection technique designed to balance detection performance with computational efficiency. The proposed method reduces the number of complex multiplications required, making it suitable for low signal-to-noise ratio (SNR) environments while maintaining adequate detection accuracy. The methodology includes detailed system modeling to simulate the signal and noise conditions typical of 5G NR systems. The results indicate that this low-complexity PSS detection method is well-suited for practical use in 5G NR mobile stations, providing an efficient solution that aligns with the performance and resource constraints of modern mobile communication systems. The performance of this technique is tested through simulations, showing that PSS can be correctly detected at a signal-to-noise ratio (SNR) of -6 dB, meeting the performance needs. Additionally, complexity can be reduced by sacrificing some detection capability of the PSS.*

Keywords: 5G New Radio; Cell Searching; Synchronization; Primary Synchronization Signal; Secondary Synchronization Signal

1. INTRODUCTION

To meet ITU IMT-2020 requirements, the fifth Generation (5G) New-Radio (NR) mobile communication has three main pillars, including enhanced mobile broadband (eMBB), massive-machine-type communication (mMTC), and ultra reliable low latency (URLC), that support new emerging applications in various domains such as high-speed internet access, internet-of-things, and critical missions [1,2,3,4]. 5G-NR system adopts generalized orthogonal frequency division multiplexing (OFDM) with flexible subcarrier spacing (or numerology) as modulation technique for the physical layer to support both below 6GHz frequency, Frequency Range 1 (FR1: 410MHz-7.125GHz), and above 6GHz, Frequency Range 2 (FR2: 24.25GHz-71GHz) frequency [5]. FR2 is generally known as the millimeter wave (mmWave) band, offers large bandwidth for eMBB service but experiencing high free-space pathloss. To cope with loss at mmWave band, beamforming technique, achieving high array gain from large amount of antenna elements at both 5G next-generation NodeB (gNB) and mobile station (MS), is used for loss compensation as well as for extending the communication range.

In 5G cellular network, there are total of 1008 cells corresponding to 1008 physical cell identity numbers (cell ID), unique identify each cell. Fig.1 shows an example 5G cellular network layout with 9 cells (tri-sector gNB) with its own unique cell ID. In this figure, each cell transmits four beams in spatial domain. Cell ID is designed in a hierarchical manner by combining cell ID group, $N_{ID}^{(1)}$, and cell ID within the group, $N_{ID}^{(2)}$, using (Eq. 1). $N_{ID}^{(2)} \in \{0,1,2\}$ are carried by three distinct primary synchronization signals (PSS). $N_{\mathrm{ID}}^{(1)} \in \{0,1,2,\ldots,335\}$ is carried by 336 distinct secondary synchronization signals

* Corresponding author: Leakana Ouk
E-mail: oukleakana01@gmail.com ; Tel: +855-81 25 33 89

(SSSs). PSS and SSS are downlink synchronizations generated from pseudo-random sequency of maximal-length of 127 with different initial conditions [6]. PSS and SSS are physical signals generated at the physical layer and broadcasted periodically over radio interface. Cell ID denoted by N_{ID}^{cell} is computed by

$$N_{ID}^{cell} = 3N_{ID}^{(1)} + N_{ID}^{(2)} \quad \text{(Eq. 1)}$$

For exampling from (Eq.1), if $N_{ID}^{(2)} = 2$ and $N_{ID}^{(1)} = 335$, $N_{ID}^{cell} = 1007$, the maximum cell ID [7]. In this paper, 5G cell and gNB are used interchangeably.

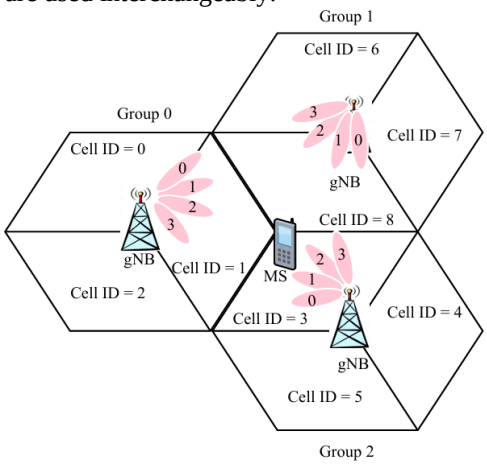

Fig.1. 5G Cellular Network.

To communicate with the 5G cellular network and access useful data, an MS is required to successfully perform the initial access procedure as shown in Fig.2, in which an MS performs cell searching and selection and decodes the system information block (SIB) in the downlink. The MS selects the serving cell and camp on the unbarred cell before performing a random-access procedure using the reception of downlink synchronization signals and broadcast information from gNB. After obtaining the random-access channel (RACH) resource indicated by the SIB, an MS can transmit the random-access preamble using the RACH channel for uplink synchronization. In Fig. 2, the cell searching procedure consists of three main steps: PSS detection, SSS detection, estimation of cell ID group using received SSS, and coherent demodulation of the physical broadcast channel (PBCH) carrying the master information block (MIB). However, cell identification involves only PSS and SSS detection, implying that the MS estimates timing acquisition, numerology parameter, and cell ID of each cell using received PSS and SSS [8]. Also from Fig. 2, after successful detection of PSS, SSS is received in frequency domain for detecting cell ID group, $N_{ID}^{(1)}$, by constructing cross-correlation the received SSS with all the possible local-generated 336 SSSs to calculate total cell ID (N_{ID}^{cell}).

PSS, SSS, and PBCH symbols are transmitted using 20 physical resource blocks (PRBs) in the frequency domain and 4 consecutive OFDM symbols in the time domain, which forms a synchronization signal block (SSB). 20 PRBs with 4 consecutive OFDM symbols require 3,840 resource elements (REs) [9,10], where PSS is mapped to only 144 REs corresponding to 12 PRBs with zero padding on both sides. To facilitate coherent demodulation of PBCH data symbols, downlink demodulation reference symbols (DMRS) are transmitted within the SSB by interleaving with PBCH data symbols. OFDM signals generated for an SSB support 4 numerologies values, i.e., $\mu = 0, 1, 3, 4$. The subcarrier spacing generated for each numerology is $\Delta f_{\mu} = 2^{\mu} \cdot \Delta f_{\text{LTE}}$, where $\Delta f_{\text{LTE}} = 15\text{kHz}$. Numerologies $\mu = 0, 1$ are used for frequencies below 6 GHz, and the others for frequencies above 6 GHz, to reduce the effect of Doppler shift. At the initial acquisition, the MS has no knowledge of the numerology of the gNB, μ, timing, cell ID within the group, $N_{ID}^{(2)}$, and the carrier frequency offset (CFO) value caused by mobility and the mismatch of oscillators between gNB and the MS.

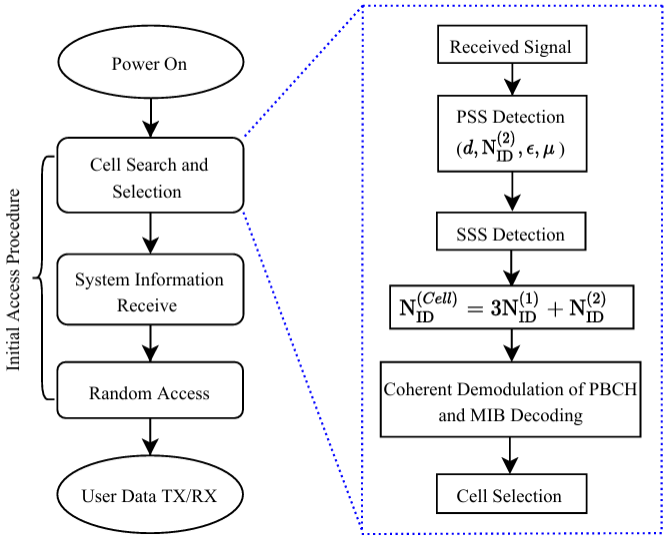

Fig. 2. Initial Access Procedure and Block of PSS Detection

The block of PSS detection illustrates the process flow for estimating synchronization parameters in a 5G NR (New Radio) system, specifically focusing on detecting the Primary Synchronization Signal (PSS). The process begins with the transmission of a signal from the base station, which includes the PSS. As the signal propagates through the wireless channel, it experiences impairments due to fading, where multipath propagation causes variations in amplitude and phase. Additionally, the signal is affected by Additive White Gaussian Noise (AWGN), representing random noise introduced during transmission. The received signal, now degraded by fading and noise, undergoes PSS detection, where the system identifies the PSS sequence to extract essential synchronization information. Finally, the system estimates the necessary synchronization parameters, such as timing offset, frequency offset, and physical layer cell identity (PCI), enabling the MS to synchronize accurately with the base station.

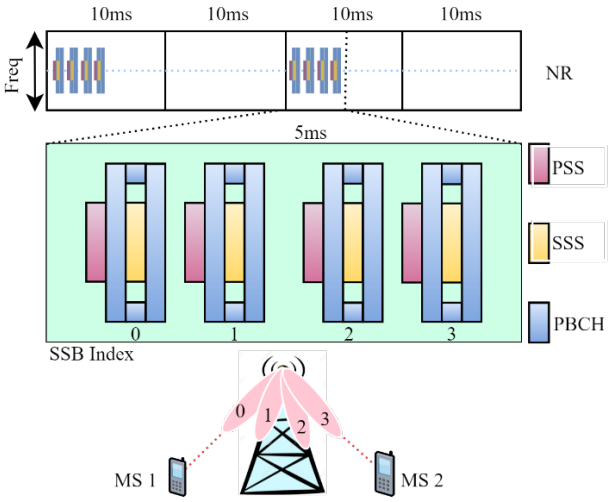

Fig. 3. SSB Burst and index mapping

This paper focuses on low-complexity PSS detection, which is a crucial step at the initial stage or when synchronization is lost. PSS detection should be efficient with low-computational complexity, thereby allowing an MS to perform cell searching quickly and less frequently, thereby prolonging the MS's battery life. By exploiting existing algorithms in a proper way, two methods (Method 1 and Method 2) with different computational complexities are formed to detect the four parameters (timing, numerology, cell ID within cell ID group, CFO) using the received PSS signal and/or SSB signals. To our best knowledge, Method 1, referred to as the conventional method in this paper, is straightforward due to the direct application of PSS cross-correlation and has been investigated similarly with different interpretations in other papers [11,12]. Methods 2 with significantly complexity reduction is proposed by exploiting the recursive calculation of the repeated information within the CP region before applying PSS cross-correlation. The rest of this paper is organized as follows: Section 2 discusses signal modeling and PSS signal generation and provides PSS detection procedures and their analysis. Section 3 illustrates performance analysis via MATLAB simulation. Finally, Section 4 concludes the paper.

2. METHODOLOGY

2.1 System Modeling

In 5G-NR system, the radio frame structure is 10ms divided into 10 consecutive subframes with duration of 1ms. Each subframe is managed into slots with 14 OFDM symbols within each slot. Each OFDM symbols consists of cyclic prefix (CP), the copied sampled from the tails of the OFDM signal and OFDM signal itself with the duration of $T_\mu = 1/\Delta f_\mu$ second [13]. The duration of CP, denoted as T_{CP}, depends on the position of OFDM symbol within each subframe, i.e., $l \in \{0,1,\dots,14 \cdot N_{\text{sl}}^{\text{sf}} - 1\}$, where $N_{\text{sl}}^{\text{sf}} = 2^\mu$ is the number of slots per subframe. For $l = 0$ and $l = 7 \cdot 2^\mu$, $T_{\text{CP}} = (144\kappa \cdot 2^{-\mu} + 16\kappa)T_c$, otherwise, $T_{\text{CP}} = 144\kappa \cdot 2^{-\mu} \cdot T_c$, where $\kappa = 64$, and $T_c = 1/N_{\text{f}} \cdot \Delta f_{\max}$, is time unit in 5G-NR system with $N_f = 4096$, $\Delta f_{\max} = 480$kHz. For example, $\mu = 0$, $\Delta f_0 = \Delta f_{\text{LTE}} = 15$kHz, $N_{\text{sl}}^{\text{sf}} = 1$ slot in each subframe. The OFDM symbol period, $T_0 = 66.66$ µs, $T_{\text{CP}} = 5.21$ µs for $l = 0,7$, otherwise, $T_{\text{CP}} = 4.69$ µs. Thus, the duration of one subframe is $T_{\text{sf}} = 14 \times 66.66 + 2 \times 5.21 + 12 \times 4.69 = 1$ms [14]. Table 1 lists the calculated OFDM parameters for each numerology value for normal CP operation mode, common operation in 5G NR. The extended CP is supported only for $\mu = 2$. $l_0 = \{0, 7 \cdot 2^\mu\}$ is the condition that CP length is longest within each subframe. In 5G New Radio (NR), the concept of numerology refers to the different parameter sets used to define OFDM characteristics. The key parameters that change with numerology are subcarrier spacing, OFDM symbol duration, cyclic prefix (CP) duration, and the number of slots per subframe. From this Table 1, the OFDM duration is shrinking as the numerology increases, implying that number of OFDM symbols increase proportional to number of slots within subframe.

Table 1. OFDM parameters

μ	Δf_μ [kHz]	T_μ [µs]	T_{CP}[µs] $l \neq l_0$	T_{CP} [µs] $l = l_0$	$N_{\text{sl}}^{\text{sf}}$
0	15	66.66	5.21	4.69	1
1	30	33.33	2.60	2.34	2
2	60	16.66	1.30	1.17	4
3	120	8.33	0.65	0.59	8
4	240	4.16	0.32	0.29	16

Owing to beam sweeping mechanism in 5G-NR system, PSS composed in SSB is transmitted in burst as time multiplex within 5ms corresponding to the number of beams determined by 3GPP technical specification [15]. Each SSB index is mapped to one spatial beam depicted in Fig. 2 from each gNB. As shown in Fig. 3, 4 SSBs corresponding to 4 beams sweeping over time are transmitted within 5ms, and the SSB burst repeats every 20ms of the radio frame. At power-on mode, the MS might scan within the 20ms period in order to guarantee the correct detection of timing and frame alignment. PSS is generated from M-sequence with maximal-length of 127 in the frequency domain.

$$d_{\text{PSS}}(p) = 1 - 2x(m_p) \qquad \text{(Eq. 2)}$$

where $m_p = (n + 43N_{ID}^{(2)}) \bmod 127$ for $0 \le p < 127$, and the 7-degree polynomial of M-sequence is given by $x(i+7) = (x(i+4) + x(i)) \bmod 2$, where the initial condition [x(6) x(5) x(4) x(3) x(2) x(1) x(0)] = [1 1 1 0 1 1 0] [16]. The mapping of PSS in the frequency domain is shown in Fig. 4 before OFDM modulation. Due real-value of PSS in frequency, the time-domain PSS has symmetric property, allowing one to use time-domain autocorrelation for PSS detection. However, it is not interest of this paper because it does not allow to the recursive implementation, the key for complexity reduction.

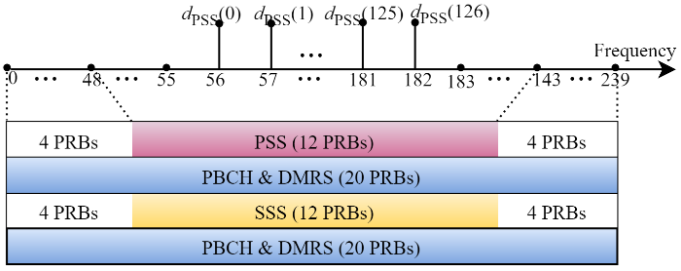

Fig. 4. PSS Mapping in frequency domain

The received discrete-time signal, $y(n)$, at an MS with a single antenna under multipath environment is given by

$$y(n) = \sum_{c=0}^{C-1}\sum_{l=0}^{L-1} e^{j\frac{2\pi}{N}\epsilon_c n} h_c(l)x(n-l) + z(n) \qquad \text{(Eq. 3)}$$

where C, L, and N denote the number of neigboring cells including serving cell, the number multipath components, and the size of fast Fourier tranfrom (FFT) used as an OFDM modulator, respectively. The power delay profile (PDP) with limited number of multipath components is determined by the 3GPP standards. Here, ϵ_c and $h_c(l)$ denote the normalized Doppler shift, the combination of both fractional and integer values, for c-th cell and l-th channel tap/coefficient of the c-th cell, respectively. It is assumed that all multipath components experience the same Doppler shift, which simplifies the simulation model. $x(n)$ and $z(n)$ denotes the transmitted signal can be either SSB signal or data and additive white Guassian noise, respeectly.

Under single-cell environment with flat fading, the receive signal is simplified as $y(n) = e^{j\frac{2\pi\epsilon}{N}n} h_c(l_0)x(n-l_0) + z(n)$, where l_0 is an arbitrary sample delay in discrete time, generally normalized to zero. The transmitted baseband PSS signal, $x(n)$, generated with 256-point inverse FFT (IFFT) of the $X_{\text{PSS}}(k)$ mapped in Fig. 4 is given by

$$x(n) = \frac{1}{N}\sum_{k=0}^{N-1} X_{\text{PSS}}(k) e^{j\frac{2\pi}{N}kn} \qquad \text{(Eq. 4)}$$

The $X_{\text{PSS}}(k)$ is obtained by performing N-piont FFT shift operation on the mapped PSS sequence in Fig. 4, and PSS signal is generally generated in association with $N_{ID}^{(2)}$. Thus, (Eq. 4) also allows MS generate time-domain PSS locally for each value of $N_{ID}^{(2)}$.

2.2 PSS Detection Procedure

This section describes and analyze the PSS detection method (Method 1 and Method 2). Method 1 shown in Fig. 5 allows to estimate the four parameters in loop manner for all possible hypotheses, although the flow chart is shown in a linear fashion. In this method, the received signal is oversampled at the rate of at least 61.44 MHz to support the largest SCS ($\mu = 4$) for PSS signal transmission. The received discrete-time signal is buffered for processing in the next steps, including decimation into lower rate and pre-compensation of integer CFO before constructing PSS cross-correlation with local-generated PSS. Here, due the lack of no fractional CFO estimation and compensation, the performance of PSS correlator is suffering from the effect of inter-channel interference in an OFDM system. For serial processing, each decimated signal is processed three times in CFO Compen. Block for three hypotheses of integer CFO, and each pre-compensated signal is correlated three times in PSS correlator block for three hypotheses of $N_{ID}^{(2)}$ values. Overall, there are $4 \times 3 \times 3 = 36$ hypotheses. This leads to computational-complexity for 20 ms processing period. The decimated signal is given by

$$y_\mu(n) = y(nM_\mu) \qquad \text{(Eq.5)}$$

where $M_\mu = F_s/F_\mu$ is the decimation factor as function of numerology value, and $F_\mu = N \cdot \Delta f_\mu$ is the processing rate for each numerology. In this paper for synchronization block the input sampling rate is $F_s = N \cdot 240\text{kHz}$ with FFT size $N = 256$. The decimation is given by

$$M_\mu = \frac{F_s}{F_\mu} = \frac{\Delta f_\mu}{240\text{kHz}} = 2^{-\mu} \cdot \frac{240\text{kHz}}{15\text{kHz}} = 2^{-\mu+4} \qquad \text{(Eq. 6)}$$

For $\mu = \{0,1,3,4\}$, $M_\mu = \{16,8,2,1\}$. From (Eq. 6), the decimation factor needs to be integer value while sampling rate, F_s can be larger than 61.44 MHz. The integer CFO compensation block is processed by using (Eq. 7)

$$y_\mu^\epsilon(n) = y_\mu(n) e^{-\frac{j2\pi\epsilon}{N}n} \qquad \text{(Eq. 7)}$$

From (Eq. 7), the range of integer CFO, $\epsilon = \{-1,0,1\}$, is chosen based on the operated oscillator plus the maximum Doppler shift caused by relative velocity between gNB and the MS. The total normalized CFO, $\epsilon_T = \epsilon + \epsilon_f = F_D/F_s$, F_D is the total CFO value. The compensated signal for each decimated signal is correlated with the local PSS generated for each $N_{ID}^{(2)}$ by

$$R(\mu,\epsilon,u,d) = \frac{1}{N}\sum_{n=0}^{N-1} y_\mu^\epsilon(n+d)x_u^*(n) \qquad \text{(Eq. 8)}$$

In (Eq. 8), $u = \{0,1,2\}$ is used instead of $N_{ID}^{(2)}$ for sake of notational simplicity. The joint detection of numerology, integer CFO, cell ID within cell ID group, and timing is obtained by selecting the maximum value of correlation by

$$(\hat{\mu},\hat{\epsilon},\hat{u},\hat{d}) = \arg\max_{\mu,\epsilon,u,d} |R(\mu,\epsilon,u,d)| \qquad \text{(Eq. 9)}$$

In method 2, the decimated signal is first processed in the autocorrelation block for course timing acquisition, the OFDM boundary between each OFDM symbols, and fractional CFO value. The autocorrelation metric is given by

$$R_\mu(d) = \sum_{b=0}^{B-1}\sum_{n=0}^{N_{\text{CP}}-1} y_\mu(n+d+bN_{\text{T}}) y_\mu^*(n+N+d+bN_{\text{T}}) \qquad \text{(Eq. 10)}$$

(Eq.10) computes autocorrelation value accumulated over B CP blocks, and $N_T = N + N_{CP}$ is the length OFDM symbol signal plus CP interval. $R_\mu(d)$ produces plateau over small region of CP block, resulting in inaccurate OFDM boundary. The PSS boundary is estimated by

$$\hat{d}_\mu = \arg\max_d \left|R_\mu(d)\right| \quad \text{(Eq. 11)}$$

From (Eq. 11), the scanning range of discrete time, d, can be within an OFDM symbol ($0 \le d \le N_T$) if there exist data transmission for every OFDM symbols. For lean transmission, gNB transmits only SSB burst if there is no data for transmission. In this case, the value of d needs to be within range to 20ms. Also, from (Eq. 10), $\hat{d}_\mu$ can be detected once the autocorrelation value $\left|R_\mu(\hat{d}_\mu)\right|$ exceeds a predefined threshold value (γ_{th}), that is, $\left|R_\mu(\hat{d}_\mu)\right| \ge \gamma_{th}$. In this way complexity is less than scanning over long periods of time if the condition is met. In this paper, (Eq. 11) is considered due to predefined threshold value requires practical modeling of background noise plus level of interfering signal. It should be noted that the fractional CFO, ϵ_f, can estimated from correlation at estimated OFDM boundary by

$$\hat{\epsilon}_f = \frac{1}{2\pi}\text{angle}\left(R_\mu(\hat{d}_\mu)\right) \quad \text{(Eq. 12)}$$

From Fig. 6 and using (Eq. 7), compensation block can mitigate the effect of CFO using the total CFO, $\epsilon_T = \epsilon + \hat{\epsilon}_f$. After obtaining the OFDM boundary, PSS cross-correlation is constructed over shorter scanning intervals for all the possible OFDM symbols during 20ms. In another case, PSS can be detected once the cross-correlation exceeds a predefined threshold, which not the focus of the paper due to practical limitation in estimating the threshold value. All the four parameters can be jointly obtained by

$$(\hat{\mu}, \hat{\epsilon}, \hat{u}, \hat{d}) = \arg\max_{\mu,\epsilon,u,d} \max\{|R_s(\mu, \epsilon, u, d)|\} \quad \text{(Eq. 13)}$$

(Eq. 14) $R_s(\mu, \epsilon, u, d)$ is computed for all possible OFDM symbols, $s \in \{0,1, \dots, S-1\}$ with S being the number of OFDM symbols to be processed. Detonating, $y^{\epsilon}_{\mu,s}(n)$, they received signal for s-th symbol, the cross-correaltion in (Eq. 13) is given by

$$R_s(\mu, \epsilon, u, d) = \frac{1}{N}\sum_{n=0}^{N-1} y^{\epsilon}_{\mu}(n+d)x^*_u(n) \quad \text{(Eq. 14)}$$

with $-D_0 + sN_T \le d \le D_0 + sN_T$, and D_0 is smaller than the CP interval owing to the high accurate detection of $\hat{d}_\mu$.

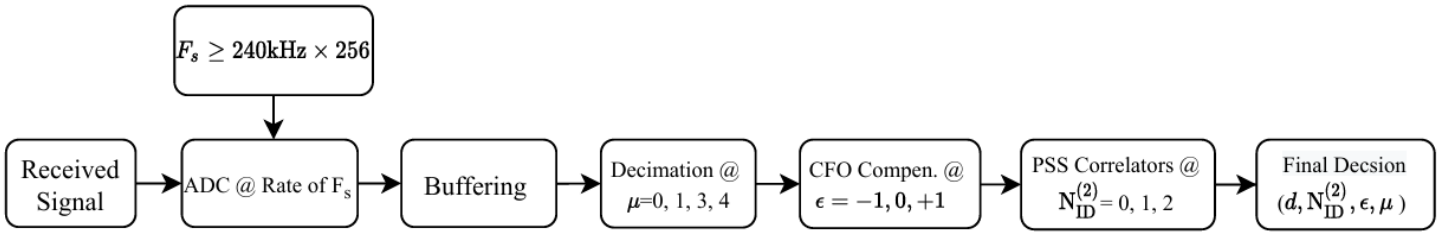

Fig. 5. Method 1: PSS detection using direct PSS cross-correlation

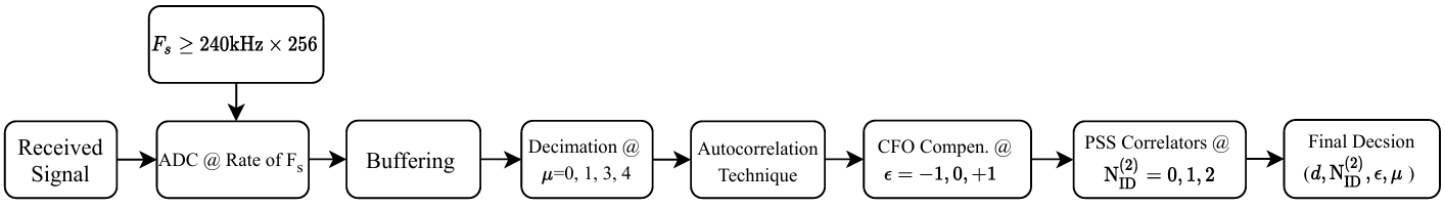

Fig. 6. Method 2: PSS detection with aid of CP-based autocorrelation

The complexity of method 2 is significantly reduced due to the recursive implementation of (Eq. 10). For example, for $B = 1$, (Eq. 10) is implemented recursively by

$$R_\mu(d) = R_\mu(d-1) + y(d)y^*(d+N) - y(d-1)y^*(d+N-1) \quad \text{(Eq. 15)}$$

where $d > 0$ and $R(0)$ is initially computed using (Eq. 10) by setting $B = 1$, and $d = 0$. In (Eq. 15), there is 2 number of complex multiplications for one execution of d, excluding the complexity of initial computation, $R_{\text{CP}}(0)$ [17]. For B accumulative blocks for noise reduction, the complexity is increased by B times of Eq (15).

Complexity analysis for both methods is considered by counting the number of complex multiplications, corresponding to 4 real-number multiplications. The computational power is dominant to the number of complex multiplications rather than number of additions. Number of complex multiplications of method 1 is given by

$$C_{\text{M1}} = (2+9N)\sum_{i=0}^{3} N^i_{\text{sap}} \quad \text{(Eq. 16)}$$

where $N = 256$ and $N^i_{\text{sap}} = TF_i$ denote the FFT size and number of samples, respectively. Here, T and F_i denote the time interval of received signal to be processed and the sampling frequency for each numerology, i.e., i =0, 1 for $\mu = \{0, 1\}$ and i =2, 3 for $\mu = \{3, 4\}$. For method 2 with direct calculation, the number of complex multiplications is given by

$$C^{\text{Di}}_{\text{M2}} = BN_{\text{CP}}\sum_{i=0}^{3} N^i_{\text{sap}} + 9NN_{\text{E}}\sum_{i=0}^{3} N^i_{\text{sym}} \quad \text{(Eq. 17)}$$

where $N_{\text{CP}} = 18$. N^i_{sym} is number of OFDM symbols during the received time interval, T, defined for each numerology. For duration of 1ms, $N^i_{\text{sym}} = 14 \times 2^\mu$, i.e., $i = 0,1$ for $\mu = \{0, 1\}$

and $i = 2,3$ for $\mu = \{3,4\}$. For recursive implementation, the complexity is given by

$$C_{M2}^{\mathrm{Re}} = 4BN_{CP} + 2B\sum_{i=0}^{3} N_{sap}^{i} + 9N_{\mathrm{E}}N\sum_{i=0}^{3} N_{sym}^{i} \quad \text{(Eq. 18)}$$

From Eq. (17) and (18), denotes the number of samples taking into account the estimation error from the autocorrelation block.

Table 2. Complexity Comparison of both methods

Searching	Method 1	Method 2 (Direct)	Method 2 (Recursive)
10ms	24×10^8	16×10^7	95×10^6
15ms	36×10^8	24×10^7	14×10^6
20ms	48×10^8	32×10^7	19×10^6

Table 2 lists the number of complexity comparisons required for both methods for the processing time, i.e., 10 ms, 15 ms, and 20 ms. Method 2 (recursive) is the most efficient of the three, requiring the fewest operations. It likely achieves this by breaking the problem into smaller, more manageable sub-problems, significantly reducing complexity. This makes Method 2 (recursive) the best choice for applications requiring high efficiency and low computational demands. Fig. 7 illustrates the computational complexity for both methods in all time intervals.

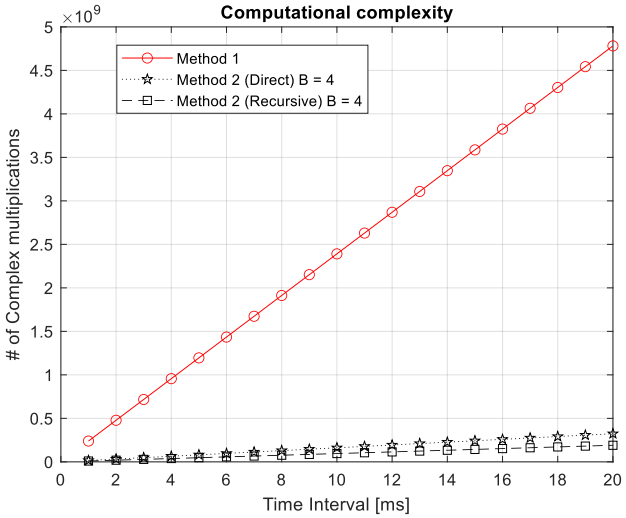

Fig.7. Complexity Comparison of both methods

3. RESULTS AND DISCUSSION

3.1 Simulation Results

In this paper, the simulation environment is a single-cell environment, although Fig. 2 is a multi-cell environment with a 9-cell layout. It is assumed that cell layout is properly planned, where the MS locates close to the serving cell so that the interfering signals from neighboring cells are weak and negligible. The OFDM parameter for the simulation is given in Table 3. Table 3 lists parameters with corresponding values for the simulation. In this table, the numerology is 0 corresponding to SCS of 15 kHz. The frequency in FR1 (up to 6 GHz) was chosen because it offers a balance between coverage and capacity, making it suitable for a wide range of deployment scenarios, particularly in urban and suburban environments where stable connections are needed despite obstacles. FR1's propagation characteristics, such as better penetration and manageable Doppler shifts, make it ideal for analyzing timing distribution. In contrast, FR2 (24 GHz to 52.6 GHz) is used for high data rate applications in dense urban areas, but it has higher path loss, shorter range, and greater susceptibility to blockages. This would require different synchronization and timing methods, making FR2 less ideal for the specific analysis focused on in this context. With a carrier frequency of 3 GHz and mobility of 500 km/h, the maximum Doppler shift caused by the motion is 1.4 kHz. By assuming that the oscillator accuracy between transmitter and receiver is 20% of the SCS, the overall frequency shift is 1.4 kHz plus. It should be noted that the accuracy of the oscillator depends on the product vendor.

Table 3. Simulation parameters

Parameters	Value
Sampling Frequency	61.44MHz
Carrier Frequency	3GHz
Numerology	0 (SCS of 15kHz)
Cyclic Prefer type	Normal CP
FFT Size	256
Resource grid	20 PRBs
SSB type	Case A
PCI number	501
Simulation environment	AWGN, 3GPP TDL Model
Mobility	0, 60, 120, 500, [km/h]

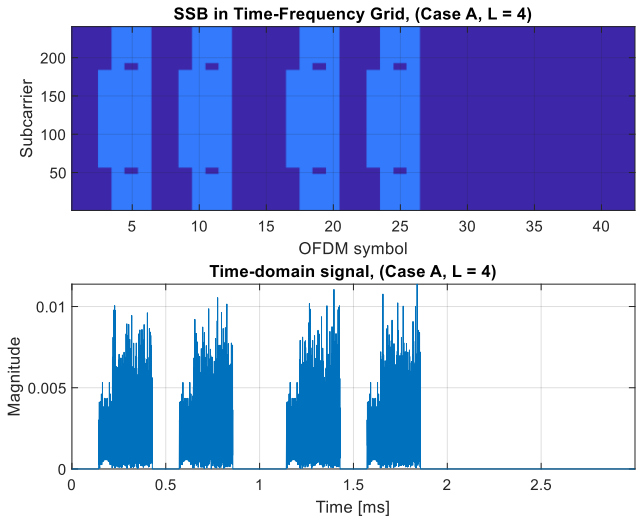

Fig.8. Transmitted SSB-Burst for Case A with SCS of 15kHz

Fig. 8 depicts the transmitted SSB burst for 3 ms, with case A consisting of 4 SSBs consecutive in the time domain. Here, there are 42 OFDM symbols in the time domain and 240 SCSs (20 PRBs) in the frequency domain. In each SSB resource grid of 960 REs, PSS and SSS occupy 280 REs including both zero padding on both sides, PBCH and DMRS interleaved in the second, third, and fourth symbols occupy 576 Res, the 4 SSBs correspond to the transmission of 4 spatial beam sweepings with indices of 0, 1, 2 and 3. In this figure, there is no user data transmission. Fig. 9 illustrates the received signal during 3 ms for a user under beam index 0 at the sampling rate given in Table 3, the strongest beam.

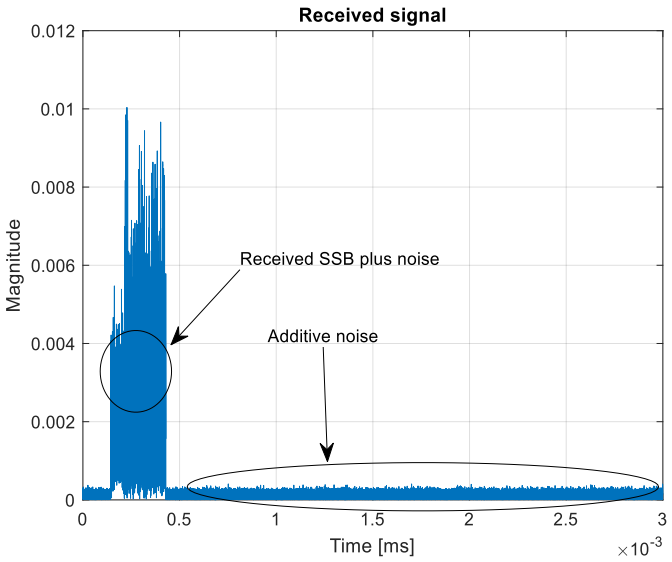

Fig.9. Received SSB-Burst for Case A with SCS of 15kHz

From Fig. 9, it is assumed that the SNR value is 30 dB, and the sidelobes contributing from beam index 1, 2, 3 are small and negligible. After receiving the SSB index 0, only a noisy signal appears: additive white Gaussian noise (AWGN). It should be noted that in the simulator, only baseband signal is considered. The object of the PSS detection is to be able to estimate the synchronization parameters correctly upon receiving the SSB plus additive noise.

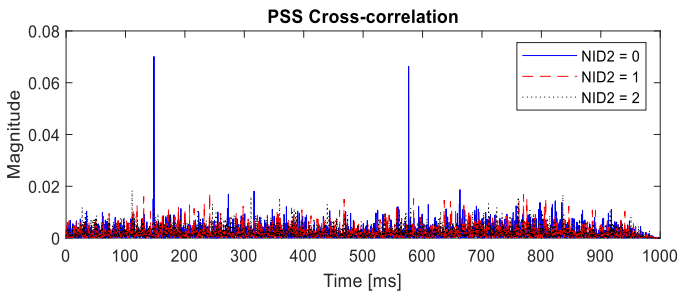

Fig. 10. PSS cross-correlation at SNR of -6dB.

It is shown in Fig. 10 that the local PSS is slide from left to right, and significant peak value (highest peak) are produced when local PSS is perfectly matched with the transmitted SSB-Burst in time-domain signal (see Fig. 8). Also in Fig. 10, there are two significant peaks appear within 1ms resulting from the matching between local PSS with the PSSs transmitted the two SSBs. From Fig. 10, timing index can be declared for the selected numerology and cell ID group so that the parameters can be obtained jointly. One can also see from Fig. 10 that there is no significant peak value appear for cell IDs that does not match with transmitted cell ID.

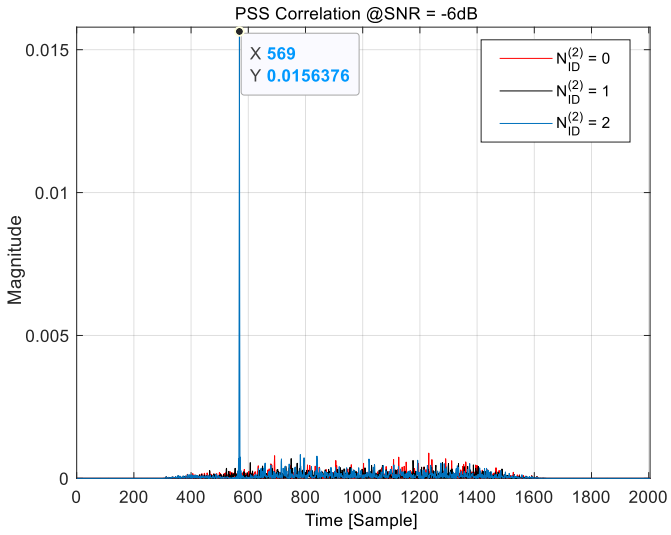

Fig. 11. PSS Correlation of method 1 for $\mu = 0$

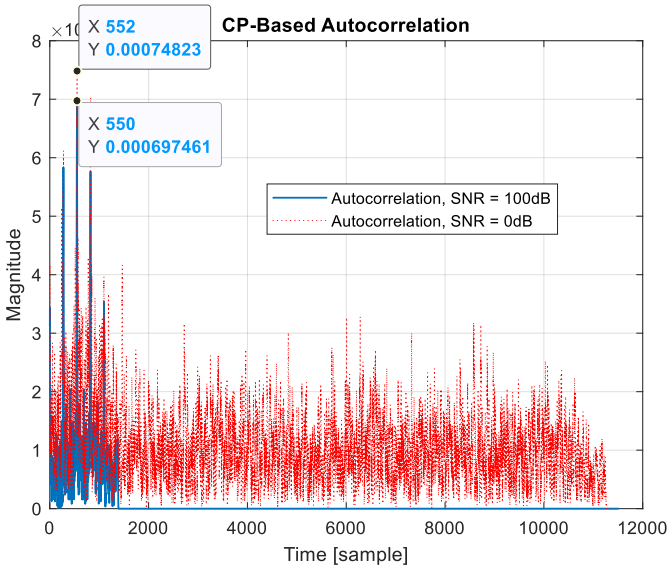

Fig. 12. Autocorrelation metric of method 2 for $\mu = 0$

It is shown in Fig. 12 that the local autocorrelation metric of method 2 is slid from left to right sample by sample, and significant peak values (highest peak) are produced when local autocorrelation. In Fig. 12, there are many single peaks because it is an autocorrelation metric; there are two significant peaks that appear within autocorrelation at SNR = 100 dB and SNR = 0 dB. From Fig. 12, a timing index can be declared for the selected numerology so that the parameters can be obtained jointly.

Fig. 11 and 13 show the timing distribution acquired at the SNR of -6 dB and the PSS correlation of method 1 for under 2000 trials, respectively. From Fig. 13, the timing distribution of method 1 is almost 50% at the first SSB corresponding timing index of {1,2} + 14 *{0,1}. For carrier frequencies smaller than or equal to 3 GHz, n = 0, 1 and another 20% at the second SSB, corresponding to a timing index of {1,2,8,16} + 14 *{0,1,3,4} For carrier frequencies 3 GHz smaller than fc smaller than or equal to 6 GHz. One can also see from Fig. 13 that there is no timing error at the SNR of -6 dB because the PSS correlation of method 1 for is = 2 at this SNR value (see Fig. 11). From the technical specification, performance satisfaction is = 2 at the SNR of -6 dB, implying that the synchronization can achieve as low a SNR as -6 dB. However, it is beneficial but not necessary to be decodable at -6 dB for user data. Although it is not shown in this Fig. 11 and Fig. 13, performance under multipath fading and Doppler shift will be poorer because the PSS correlation value decreases as Doppler increases. In this diversity, techniques need to be considered in order to improve the performance. The diversity technique is shown in Fig, 15 of this paper.

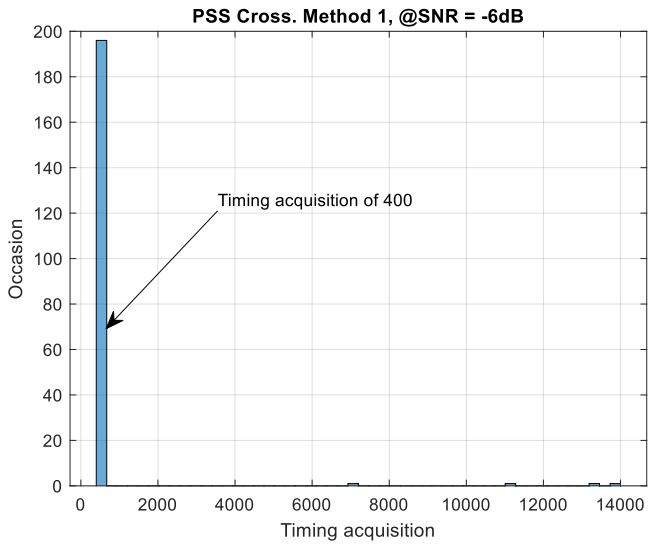

Fig. 13. Timing distribution of method 1

Fig. 14 shows timing acquisition of 500, or simulations resulted in a timing acquisition value of 568. This uniformity implies that the method is highly accurate and consistent in acquiring the correct timing at this specific value. From Fig. 14, the concentration is concentrated around a precise value (568); this suggests that Method 2 has high accuracy in timing detection with very little variation or error. The result shows that in 500 trials, the method reliably detected the timing at the same point every time. In summary, in Fig. 14, the timing distribution of method 2 is highly reliable, accurate, and consistent in detecting or acquiring the timing at a specific point (around 568).

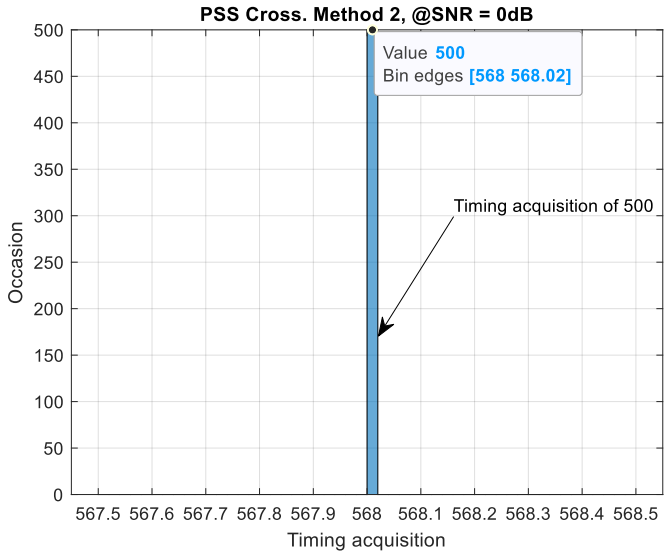

Fig. 14. Timing distribution of method 2

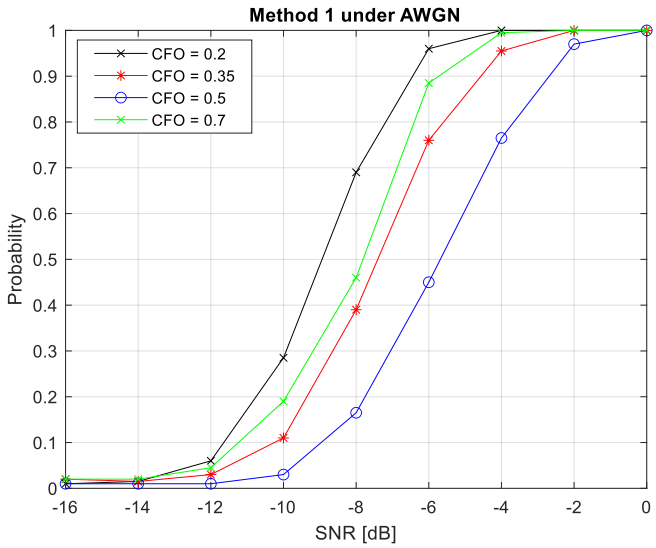

Fig. 15. Probability detection of method 1 ($CFO = 0kHz, 12kHz, 24kHz, 60kHz$)

Fig. 15, show the performance of signal detection in terms of probability is highly dependent on the SNR and CFOs. For

the method 1 the CFO values, (i.e., 0.2, 0.35, 0.5, 0,7) at lower CFO values (e.g., 0,2) the probability of detection is higher at lower SNR levels, indicating better performance. As CFO increases (e.g., 0.7), the detection probability decreases at the same SNR, indicating that larger frequency offsets make detection more challenging. The threshold SNR value increases as CFO increases. the performance of signal detection in terms of probability is highly dependent on the SNR and CFO. Lower CFO values allow for better detection at lower SNRs, while higher CFO values require a higher SNR to achieve the same detection probability. This is crucial in systems like 5G NR, where precise synchronization and detection are critical, and CFOs can significantly impact performance.

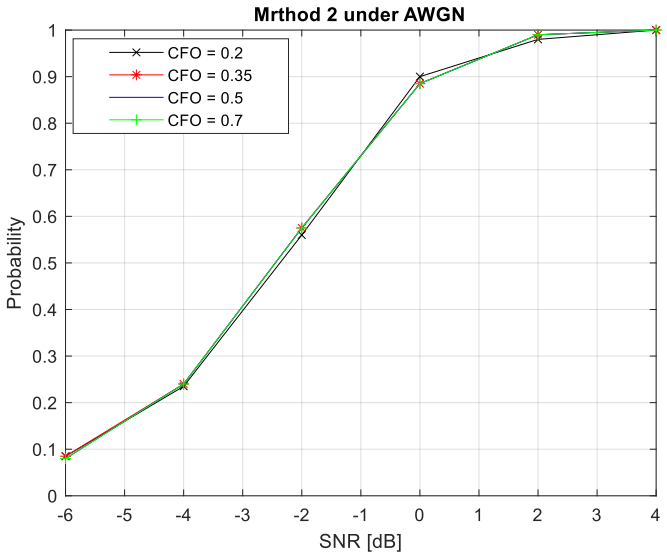

Fig. 16. Probability detection of method 2 ($CFO = 0kHz, 12kHz, 24kHz, 60kHz$)

In this figure 16, illustrates the detection probability improves with increasing SNR and shows that the impact of varying CFO values within the range provided is relatively small, as all curves follow a similar trend. At lower SNR values (e.g., -6 dB to -4 dB), the detection probability is low across all CFO values. As SNR increases (e.g., 0 dB and above), the detection probability rapidly increases and saturates close to 1, indicating reliable detection across all CFO values. This is indicative of a detection method 2 that is relatively robust to CFO variations.

4. CONCLUSIONS

In this paper, the study explored a low-complexity detection technique for the Primary Synchronization Signal (PSS) in 5G New Radio (NR) terrestrial cellular systems. In Section 1, we discussed the signal modeling and PSS generation, providing a detailed analysis of the PSS detection procedure. The analysis highlighted the method's ability to maintain robust detection performance in the presence of noise and Doppler effects while reducing computational complexity. Section 2 presented a performance analysis using MATLAB simulations. The results demonstrated that the proposed detection technique could reliably identify the PSS at signal-to-noise ratios as low as -6 dB, meeting the stringent performance requirements of 5G NR systems. Additionally, the method achieved a significant reduction in computational complexity, making it a viable solution for mobile stations with limited processing power. Future research should focus on extending this low-complexity detection technique to handle more complex scenarios, such as multi-cell environments and varying mobility conditions. Further investigation into hardware implementation and optimization could also enhance real-time processing capabilities. Moreover, integrating this technique with other synchronization and cell-search methods in 5G NR systems could provide a more comprehensive and efficient synchronization framework.

ACKNOWLEDGMENTS

The authors would like to thank the financial support under the Cambodia Higher Education Improvement Project (Credit No. 6221-KH) for the sub-project of HEIP-ITC-SGA#02 at the Institute of Technology of Cambodia (ITC) and co-funded by the National University of Battambang (NUBB).

REFERENCES

[1] A. Sophia, "5G NR: Physical channels and modulation," 3GPP TS 138.211. Ver 15.3.0, Re 15, 2018.
[2] A. Sophia, "5G NR: Physical channels and modulation," 3GPP TS 138.211. Ver 15.10.0, Re 15, 2022.
[3] A. Sophia, "5G NR: Multiplexing and channel coding," 3GPP TS 138.212. Ver 16.2.0, Re 16, 2020.
[4] K. Chang. W. Cho. B. Kwak. J. B. and Y. J. Ko, "Synchronization Under Hardware Impairments in Over-6-GHz Wireless Industrial IoT Systems," IEEE Internet. Things Journal, vol. 10, Iss. 7, pp. 6082–6099, 2023b.
[5] A. Sophia, "5G NR: Base Station (BS) radio transmission and reception," 3GPP TS 138.104. Ver 16.4.0, Re 16, 2020.
[6] Y. Jeon. H. Park. and E. Choi, "Synchronization and Cell Search Procedure in 3GPP 5G NR Systems," 2019.
[7] A. Ghosh. A. Maeder. A. Baker. M. and D. Chandramouli, "5G Evolution: A View on 5G Cellular Technology Beyond," IEEE Access, 3GPP (Re. 15), no. 7, pp. 127639–127651, 2019b.
[8] J. Liang. And J. Hou, "Simulation of 5G Secondary Synchronization Signal Detection," 2019b.
[9] A. Sophia, "5G NR: Physical channels and modulation," 3GPP TS 138.211. Ver 16.2.0, Re 16, 2020.
[10] A. Sophia, "5G NR: Physical channels and modulation," 3GPP TS 138.211. Ver 15.3.0, Re 15, 2018.

[11] R. Pec. J. Choi. H. Park. H. C. and Y. S. Cho, "Synchronization method for long-term evolution-based machine-type communication in low-power cellular Internet of Things," Inter Journ of Distributed Sensor Networks, vol. 12, Iss. 8, 2016.

[12] X. Li. F. Chen. Y. Zhang. and Y. Jiang, "Design and implementation of initial cell search in 5G NR systems," IEEE Xplore, pp. 39-49, May. 2020.

[13] Y. Kryukov. D. Pokamestov. and E. Rogozhnikov, "Cell search and synchronization in 5G NR," [ITM Web of conferences 30, 04007]. https://doi.org/10.1051/itmconf/201930 0 4007. 2019.

[14] D. Wang. Z. Mei. H. Zhang. and H. Li, "A Novel PSS Timing Synchronization Algorithm for Cell Search in 5G NR System," IEEE Access, vol. 9, pp. 5870–5880, January. 2021.

[15] A. Sophia, "5G NR: Multiplexing and channel coding," TSGR, 3GPP TS 138.212. Ver 16.2.0, Re 16, 2020.

[16] A. Chakrapani, "On the Design Details of SS/PBCH, Signal Generation and PRACH in 5G-NR," IEEE Access, vol. 8, pp. 136617–136637, July. 2020.

[17] Y. H. You and Y. A. Jung, "Complexity-Efficient Sidelink Synchronization Signal Detection Scheme for Cellular Vehicle-to-Everything Communication Systems," Mathematics, vol. 11, Iss. 18, September. 2023.